Vietnam Journal of Earth Sciences, 44(3), 369-394, https://doi.org/10.15625/2615-9783/17010

Vietnam Academy of Science and Technology
Vietnam Journal of Earth Sciences
http://www.vjs.ac.vn/index.php/jse

Site classification of seismic recording stations of Garhwal region of earthquake early warning system for Uttarakhand, India

Pankaj Kumar[1*], Bhavesh Pandey[2], Kamal[3], Ashok Kumar[4]

[1]*Centre of Excellence in Disaster Mitigation & Management, Indian Institute of Technology Roorkee, India*
[2]*B.T. Kumaon Institute of Technology, Dwarahat, Uttarakhand, India*
[3]*Department of Earth Sciences, Indian Institute of Technology Roorkee, India*
[4]*Department of Earthquake Engineering, Indian Institute of Technology Roorkee, India*

Received 16 September 2021; Received in revised form 11 February 2022; Accepted 07 April 2022

ABSTRACT

Site classification is vital to carry out seismic hazard analysis of a region and get the damage patterns caused by earthquakes. In the present study, the ground motion of earthquakes recorded from 2015 to 2019 at 84 sites of the seismic network array of Earthquake Early Warning System for Uttarakhand are analyzed for site classification purposes. The predominant period from the mean horizontal to vertical spectral ratio curves was estimated. The classification schemes devised by Japan Road Association and National Earthquake Hazards Reduction Program are applied to classify the sites. Along with this, two other site classification indexes schemes are also applied for classification purposes. Data winnowing techniques are used over the ground motion records to pick out desirable quality records. Conclusively, the site class with the highest recurrence rate amongst the used methods is selected as the final class for that particular site. The effect of magnitude, distance and depth on horizontal to vertical spectral ratio are described and concluded that these factors do not significantly affect the ratio curves. The average horizontal to vertical spectral ratio curves obtained for all the sites matches well with the existing literature. The classification of a few sites are verified from the classification done by other methods in recent studies. It is evident from the results that the classification done in this study matches well with them.

Keyword: Site classification, H/V spectral ratio, predominant period, Garhwal Himalaya.

1. Introduction

In the aftermath of an earthquake, some structures are often unaffected while nearby, similar structures show significant damages. One of the foremost reasons is the difference in site response characteristics within the area, as the surface layers underlying these structures behave differently during earthquakes. The study of the response of surface layers concerning the shaking of earthquakes is an essential requirement for mitigation of earthquake disasters. Drilling exploration is undoubtedly the most reliable method to study dynamic characteristics of surface layers as this accurately estimates

*Corresponding author, Email: pkumar@dm.iitr.ac.in

geotechnical properties. But boreholes require a lot of effort, money, human resources, and time in particular to study a large area.

The shear wave velocity (V_{s30}) of top 30-meter soil strata from the surface are the most widely accepted parameter for site classification and have been used in many codes, like National Earthquake Hazard Reduction Program (NEHRP) (BSSC, 2004), Universal Building Code (UBC, 1994), and New Zealand Seismic Code (New Zealand Standard, 2004). There are several methods available to estimate local site effects/site amplification, such as the traditional spectral ratio technique (Borcherdt, 1970), generalized inversion technique (Field and Jacob, 1995), the receiver function method (Langston, 1979), Nakamura's method of the spectral ratio of the horizontal and vertical component of recorded micro-tremor/ambient noise (Nakamura, 1989), and coda-wave method (Phillips and Aki, 1986). The H/V ratio of earthquake records in the S-wave window could show the overall effect of sub-surface in the frequencies caused by site responses. In contrast, the P-wave window has nothing or minimum effect of site response on frequencies of ground motion (Field and Jacob, 1995). Satoh et al. (2001) elaborate a comprehensive description of the H/V ratio of the ground motion record's various parts (P-wave, S-wave, coda). On several occasions H/V ratio does not show clear peaks; therefore, smoothing of Fourier spectra of each component of motion is required during H/V spectral ratio analysis. It smooths the spectral peaks so that the spikes corresponding to site response characteristics can be extracted from the unsmoothed spectra with many spikes. The smoothing method and extent of smoothing must be the same for the whole data set. It is desirable to have many records at a station. Any spike, which is not related to site response, can be suppressed by averaging the spectral ratio of whole available records. This smoothing process needs a significant amount of time and effort when many records at a station are available. In addition, if there are many stations to conduct H/V spectral ratio analysis. The natural frequency range of each site class provides a vital parameter to categorize sites. On the soft surface layer, horizontal motion is more prominent than vertical motion. On the other hand, at the hard surface layer, both the horizontal and vertical motions are similar in terms of maximum value and waveform (Nakamura, 2008). The H/V spectral ratio curves show the predominant period (Macau et al., 2014; Perron et al., 2018) for a site irrespective of the time, place, and season (Nakamura, 1989). In this study, H/V response spectral ratio curves are not considered the expression of the site amplification. The amplification of a site obtained from H/V spectral ratio curves is not always consistent; therefore, other approaches along with it require getting a shear wave velocity profile (Dal Moro, 2019). To get amplification and shear wave profile is not the part of the study presented in this paper.

Attenuation models are used to estimate the expected PGA under which the engineering structures are expected to expose. However, there will always be some error in estimating ground motion amplitudes from the selected model. Suppose a model is assumed to be physically correct; in that case, the amplitude error depends on the earthquake's magnitude, representation of seismic wave propagation, source to site distance and simple representation of site-effects in terms of V_{s30} or predominant period. Site conditions have a substantial effect on the motion of the ground surface. Inappropriate modeling of site effects will mislead the estimations of surface ground motion (Zhao et al., 2006). In this paper, site classification of strong ground motion recording stations in Garhwal Himalaya is carried out and studied.

2. Geological settings

Collision of the inter-continental plate boundary of India and the Eurasian plate is the genesis of the Himalayas. This collision has resulted in crustal shortening, faults/thrusts, and complex geodynamics in the Himalayan regions. The continuous underthrusting in the northward direction of the Indian plate beneath the Eurasian plate makes the Himalayan region one of the most seismically active regions of the world. Litho-tectonic features subdivide the Himalaya into four categories viz. Teyths Himalaya, Higher Himalaya, Lesser Himalaya, and sub-Himalaya or Shivaliks and their adjoining north-south plans (Pandey et al., 2021). Geodynamic complexity has exhibited in several thrust planes, and prominent are viz. Indus-Tsangpo suture zone (ITSZ), Main Central Thrust (MCT), Main Boundary Thrust (MBT), and Main Frontal Thrust (MFT). These tectonic features sub-divides the Himalayan region. The Lesser Himalaya is structurally the lowest slice and broad zone bounded by MBT in the south and MCT in the north. Geological formation of this zone is of Precambrian clastic sediments, thick Proterozoic sequence, except a narrow area of early Cambrian succession. The Higher Himalaya is a narrow zone demarcated by MCT in the south and ITSZ in the north. This region comprises the Archaean-Palaeoproterozoic sequence and is the ensemble of central crystalline and early Cambrian metasedimentary rocks. The Tethys Himalaya is the northmost subdivision of the Himalaya and is north of the higher Himalaya. The Indus-Tsangpo suture zone separates it from the Trans-Himalayan zone in the north. The MCT places high-grade gneisses (Higher Himalaya) on top of lower-grade schists (Lesser Himalaya), while the MBT juxtaposes those schists against unmetamorphosed Miocene-Pleistocene molasses (sub-Himalaya). The tectonics features present in the Garhwal region are shown in Fig. 1. Seismic sensors are installed along with the MCT and MBT (Fig. 1). The site classification of sensor locations is carried out in the present study. Detailed geological perspective of Uttarakhand is shown in Fig. 13.

3. Earthquake dataset used in H/V spectral ratio analysis

The Earthquake Early Warning (EEW) System Laboratory, IIT Roorkee, has instrumented a seismic network in the Garhwal region of Central Himalayas between Uttarkashi and Joshimath. Many geophysicists and earthquake scientists elaborated in their research that this region lies in the central seismic gap, and strong earthquake/s would probably trigger in this region soon (Mridula et al., 2014; Srivastava et al., 2015). The selection of this region for the installation of sensors was made after considering their findings (Dimri, 2013; Kumar et al., 2012). Their studies have shown that a great earthquake in Central Himalayas could generate significant ground shaking up to National Capital Region (NCR) Delhi, located nearly 200 km from MBT and 300 km from MCT (Mittal et al., 2013, 2012). The MCT and MBT are the two most active thrust planes of the Himalayas.

Under this project, instrumentation of 84 Micro-Electro-Mechanical System (MEMS) accelerometers has been done in the Garhwal region of Uttarakhand (Chamoli et al., 2019; Kumar et al., 2021). These sensors are installed on the ground floor of government-owned offices of Base Transceiver Station (BTS) of Bharat Sanchar Nigam Limited (BSNL) and Point of Presence (PoP) of State Wide Area Network (SWAN) available in the Garhwal region of Uttarakhand. The sensors send the data to the central server through dedicated leased lines in the EEW System laboratory, IIT Roorkee, and auto-update its time through the NTP server.

Figure 1 represents the location of the sensors along with the existing tectonic features in the region.

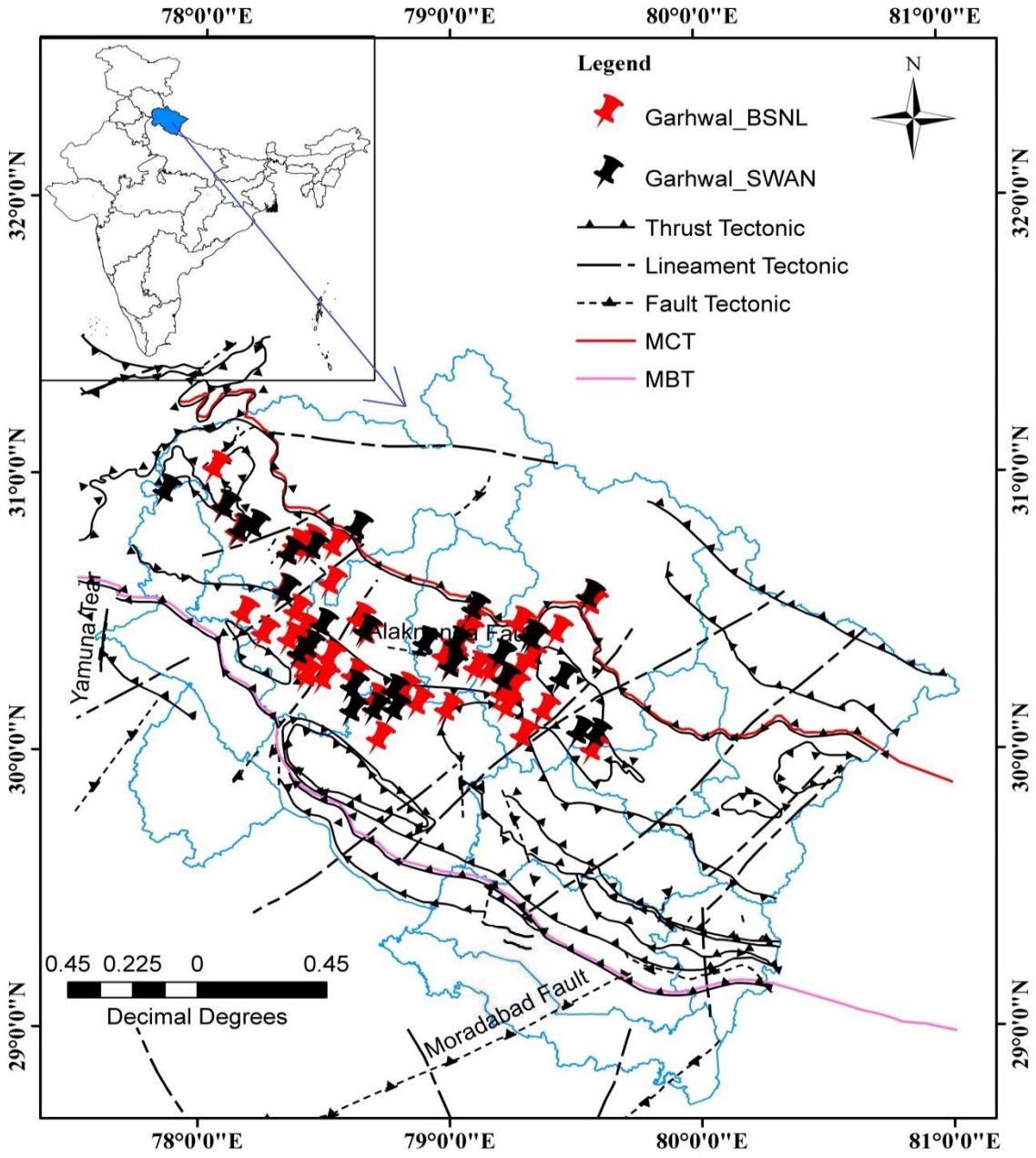

Figure 1. Location of sensors installed in Garhwal region of Uttarakhand province. The tectonic features present in the region are also shown

Table 1 represents the records of the earthquakes from 2015 to 2019 recorded at the central server. Among 38 earthquakes, 32 were originated in the instrumented region, and six occurred in the far-field region (i.e., out of the instrumented area) but recorded at the central server. Figure 2 shows the epicenter of enlisted earthquakes in Table 1. The distribution of the records is plotted as moment magnitude (M_w) versus

epicentral distances in Fig. 3. This figure clearly shows a positive correlation between earthquake magnitudes and epicentral distances. The effect of depth, magnitude, and hypocentral distances on the H/V response spectral curves do not make a significant difference and is discussed in section seven.

Table 1. The primary information of the earthquakes recorded at the central server in EEW System Laboratory, IIT Roorkee

No.	Date	Latitude	Longitude	Depth (Km)	Mag (M_w)	Region
1	18/07/2015	30.5 N	79.1 E	13	4.3	Uttarakhand
2	06/08/2015	30.3 N	79.5 E	10	2.9	Chamoli
3	29/11/2015	30.6 N	79.6 E	10	4	Chamoli
4	25/09/2016	30.5 N	78.9 E	10	3.7	Rudraprayag
5	23/11/2016	30.3 N	78.0 E	10	3.4	Distt. Dehradun
6	01/12/2016	29.8 N	80.6 E	10	5.2	Nepal-India Border Region
7	13/12/2016	30.9 N	78.0 E	5	3.4	Uttarkashi
8	19/12/2016	30.9 N	78.0 E	10	3.4	Uttarkashi
9	26/12/2016	30.8 N	77.9 E	10	3.5	Distt. Dehradun
10	10/01/2017	30.3 N	79.4 E	5	3.2	Distt. Chamoli
11	23/01/2017	30.8 N	78.2 E	10	3.5	Distt. Uttarakashi
12	03/02/2017	30.5 N	79.2 E	10	3.6	Chamoli
13	06/02/2017	30.6 N	79.0 E	10	3.6	Distt. Rudraprayag
14	11/02/2017	30.5 N	79.1 E	5	3.2	Rudraprayag
15	10/04/2017	30.7 N	78.6 E	10	3.8	Uttarkashi
16	16/04/2017	30.5 N	79.1 E	10	3.5	Rudraprayag
17	06/12/2017	30.4 N	79.1 E	30	5.5	Distt. Rudraprayag
18	14/06/2018	30.8 N	78.2 E	10	4	Uttarkashi
19	11/11/2018	29.7 N	80.6 E	10	5	Nepal-India Border
20	13/04/2019	30.9 N	78.2 E	10	2.9	Distt.Uttarkashi
21	17/05/2019	30.5 N	79.3 E	10	3.8	Distt. Chamoli
22	14/06/2019	29.6 N	80.4 E	10	3.8	Distt. Pithoragarh
23	06/07/2019	30.7 N	78.4 E	5	3.1	Distt. Uttarkashi
24	14/07/2019	30.9 N	78.2 E	10	3	Distt. Uttarkashi
25	11/09/2019	30.4 N	79.7 E	14	3.6	Distt. Chamoli
26	16/09/2019	29.6 N	80.7 E	10	4.3	Nepal-India Border Region
27	01/10/2019	30.4 N	79.3 E	10	3.3	Distt. Chamoli
28	12/11/2019	29.9 N	80.2 E	10	4.5	Distt-Pithoragarh
29	19/11/2019	29.4 N	81.2 E	33	5.2	Western Nepal
30	24/11/2019	30.4 N	79.3 E	10	3.4	Distt. Chamoli
31	07/12/2019	30.5 N	79.3 E	5	3.2	Joshimath
32	08/02/2020	29.9 N	79.7 E	20	4.7	Pithoragarh
33	26/10/2015	36.5 N	70.8 E	190	7.5	Afghanistan
34	25/12/2015	36.5 N	71.2 E	186	6.5	Hindukush-Afghanistan
35	02/01/2016	36.5 N	70.9 E	170	5.8	Hindukush-Afghanistan
36	31/01/2018	37.4 N	69.6 E	190	6.2	Afghanistan -Tajikistan Border
37	09/05/2018	36.9 N	71.3 E	96	6.1	Afghanistan-Tajikistan Border
38	24/09/2019	33.1 N	73.7 E	10	6	India-Pakistan(J & K) Border

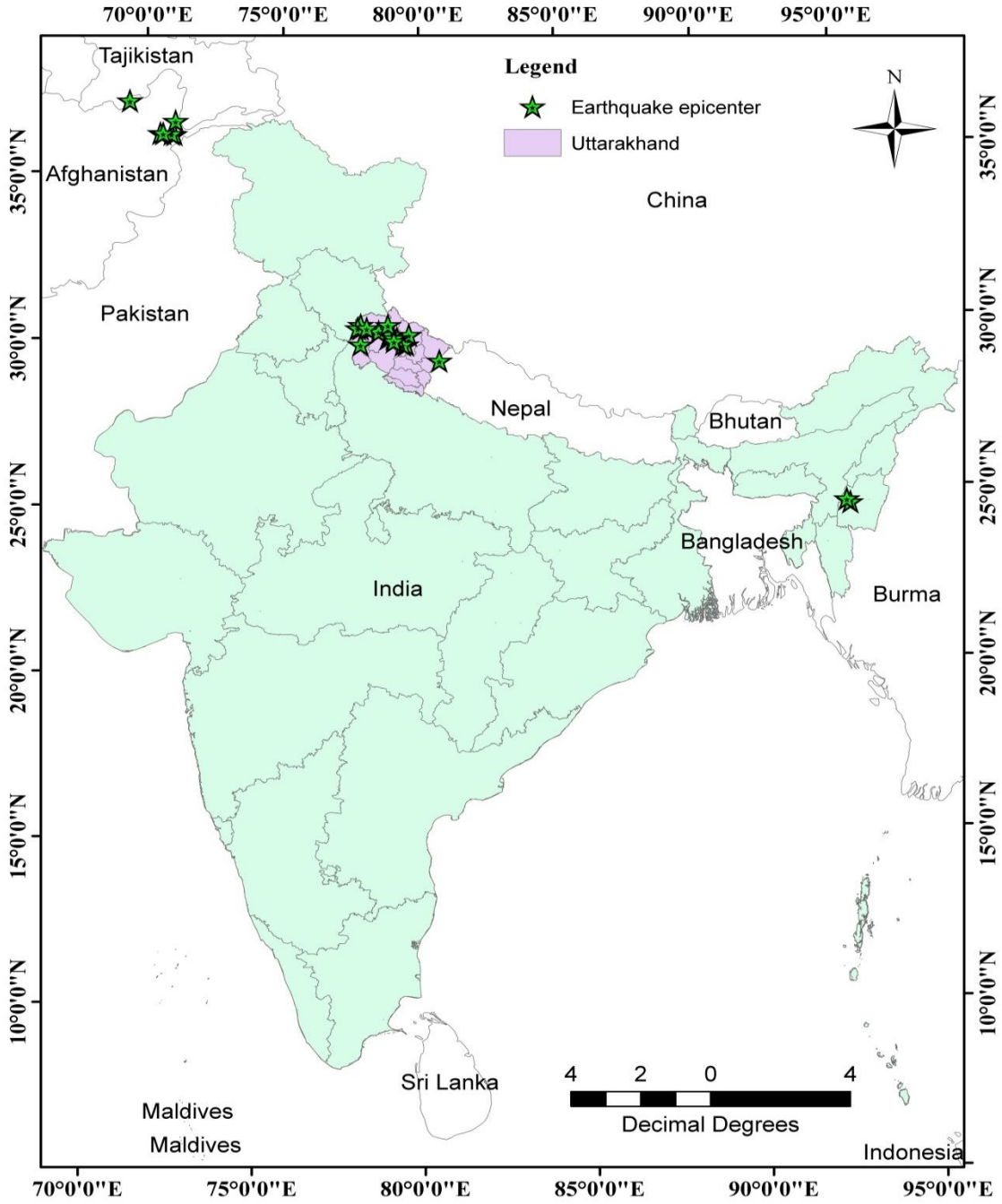

Figure 2. Representation of epicenters of the earthquakes recorded at the central server

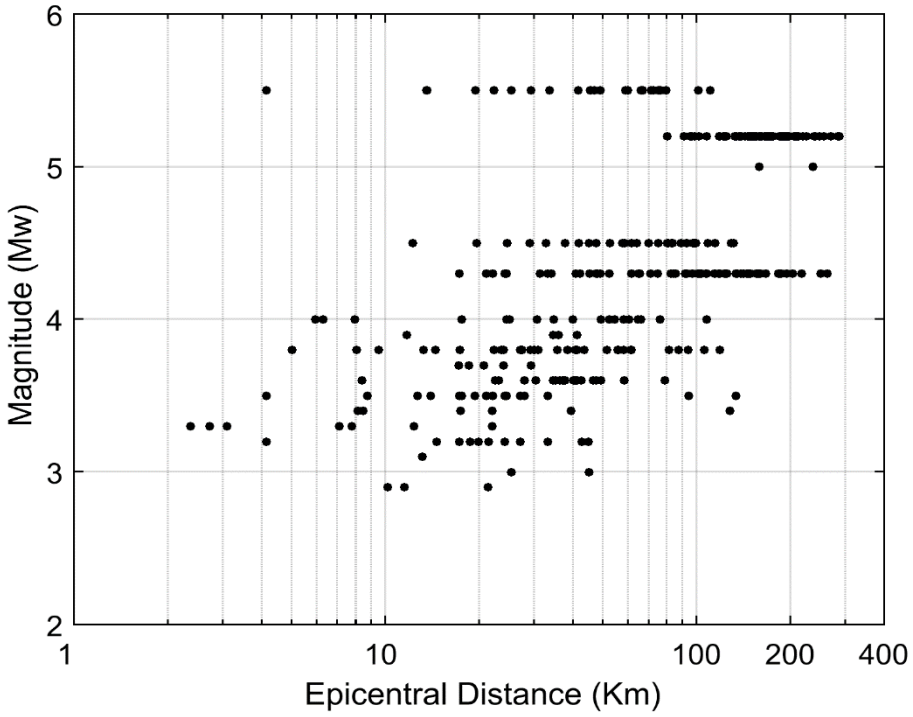

Figure 3. Relationship between magnitude and epicentral distance of the records retrieved at the central server. This relationship shows a positive correlation between these two parameters

4. Noise analysis of the records

This study created and utilized the response spectra of strong ground motion records. Noise removal techniques were applied to separate the noise from the data. The first correction of the ground motion data was to perform baseline correction to avoid low-frequency spectral noise in Fourier amplitude spectra. The recorded data was in counts and converted into gal by multiplying converting factor. If no drift exists in the record, the count fluctuates around zero. But, if this count fluctuates around some other number except zero, then the baseline correction needs to be carried out. For this, the mean value of the 20 seconds pre-event noise was considered the drift (Yu et al., 2000). This value was subtracted from the whole record. By doing so, the drift in the records was removed.

The noise influences the strong ground motion data at the low and high frequencies where the signal-to-noise ratio is low (Douglas and Boore, 2011). Hence, the cut-off frequency of the high pass filter is the key factor in removing the long period noise. Suppose the cut-off frequency is lower than the frequency of low-frequency noise. In that case, there will be a significant deviation in integrated velocity and displacement and thus the amalgamation of low-frequency spectral noise in Fourier amplitude spectra. Low-frequency information may be cropped out if the cut-off frequency is high. Therefore, selecting the cut-off frequency of the high pass filter is very important. In this work, digital bandpass Butterworth filter of order four is applied to remove the short period and long period noise from the records as implemented by Ghasemi et al. (2009). The cut-off frequency at the lower and upper bound of the bandpass Butterworth filter are taken as 0.075 Hz and 25 Hz, respectively. This cut-off frequency range is

sufficient for the required target period range of the spectral curve of 0.05 to 5 seconds. It is evident in Fig. 4 that there is a discernable difference between filtered and unfiltered acceleration at low frequencies and high frequencies. Therefore, filtering of data is required to remove undesirable frequency noises.

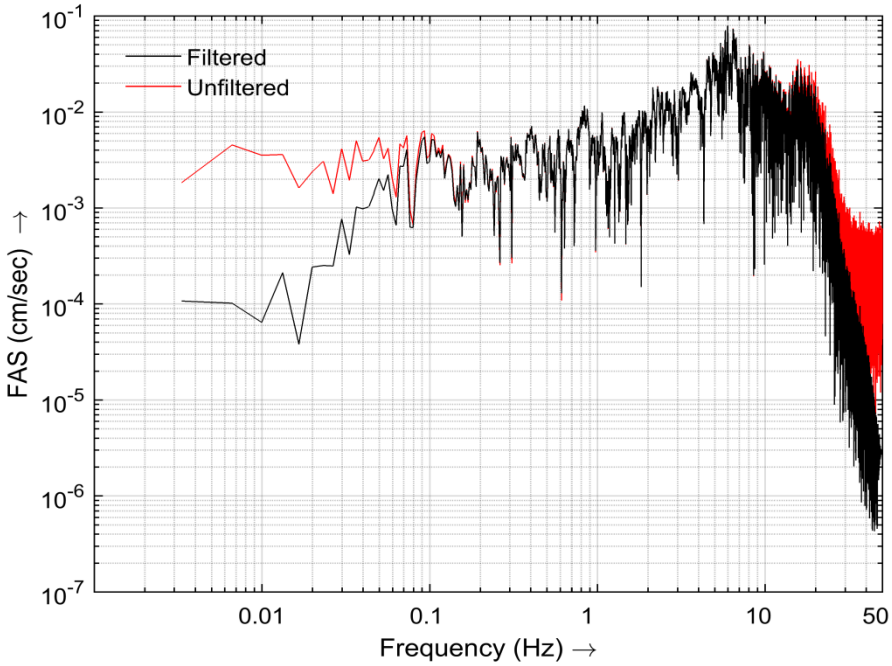

Figure 4. Shows variation in the filtered and unfiltered acceleration record of M_w 4.3 of the July 18, 2015 earthquake recorded at Tilwara station

The signal-to-noise ratio (SNR) analysis was performed to know the strength of the signal in the recorded data. Noise in the records affects the engineering parameters (e.g., response spectra, etc.). The choice to select the record is never unambiguous and depends on what is considered to be an acceptable SNR. In the present study, the predominant period of the site needs to be found out. Therefore, the higher the SNR, the more visible the predominant period could be recognized. Filtering of data improves the SNR. Dataset used in this study is digital, and it has significant pre-event and post-event records. The PPHASEPICKER algorithm was applied to find out the P-onset in the records (Kalkan, 2016), but it was observed that manually picking is better. Therefore, the P-onset time of the earthquake and the entire signal window of all the records were extracted manually. The noise window was selected from pre-event data as same length as the signal window for each individual record of each individual earthquake. The baseline correction and filtering were carried out for each record. Fourier transform of the full signal window and noise window was done, then SNR was calculated by applying equation (1) (Havskov and Alguacil, 2015).

$$SNR = 20 \times log10\left(\frac{rms(signal)}{rms\,(noise)}\right) \quad (1)$$

Described method in equation (1) is applied to each record to determine SNR. In this study, the records with an SNR ratio greater than five were selected for the site characterization purpose. The earth crust is

very complex and heterogeneous; thus, the nonlinear soil phenomena are often evident in many large earthquake events and could influence the shape of the H/V spectral ratio curve due to drift in spectral period and de/amplification of spectral ratio. The records with the large peak ground acceleration show the influence of nonlinearity behavior of soil in H/V curves (Wen et al., 1995, 2006). Therefore, to avoid the possible large variation on H/V curves, only those records with PGA<100 gals were selected in this study. To prevent the possibility of the poor quality of signals, recording with PGA< 5 gals were excluded. By doing so, improved SNR was achieved by avoiding the possible influence of noise in the H/V spectral ratio curves (Ji et al., 2017). Total 769 records from 38 earthquakes recorded at 84 stations were processed with a bandpass filter to eliminate long-period ground motion with a frequency less than the corner frequency and to remove high-frequency noise.

5. Methodology

The H/V spectral ratio curve method uses a ratio of Fourier spectra of horizontal to vertical motion of microtremors to evaluate the site classification. It is based on the assumption that the soil amplification characteristics are retained in horizontal motions. In contrast, path and source characteristics of seismic waves are retained in both horizontal and vertical components of motions (Nakamura, 1989). This method was applied on strong motion records picked by JMA-87-type accelerometers in Japan and concluded that Nakamura's approach is also applicable to the strong ground motion records. The horizontal to vertical Fourier spectrum ratio remains stable irrespective of earthquake magnitude, source to site distance, depth, and stated that this H/V spectral ratio could be a valuable tool for site classification (Yamazaki and Ansary, 1997). The H/V spectral ratio of strong motion is a stable method for site classification (Zare et al., 1999). Procedure to create a H/V spectral ratio curve can be described as follows:

Step 1. All the records recorded at a station must be of the same time length.

Step 2. Apply Fast Fourier Transform (FFT) on horizontal and vertical motion components.

Step 3. Apply Konno and Ohmachi smoothing on each component by taking bandwidth parameter 'b' 20 (Konno and Ohmachi, 1998).

Step 4. There are two-component of horizontal motion. So, the geometric mean of both components would be a resultant horizontal component.

$$A_{HR} = sqrt(A_{EW} * A_{NW}) \quad (2)$$

Step 5. Calculate the predominant period and amplitude magnification corresponding to the peak of the H/V spectral ratio curve.

Sensor at a station records many earthquakes triggered in the instrumented region; thus, there is more than one record at each station. The average of all H/V spectral curves provides good results and averages abrupt noise in the data. Thus, the H/V spectral ratio (HVSR) at each station can be determined as:

$$(HVSR)_j = \frac{\sum_{i=1}^{N_i} \frac{H}{V}}{N_i} \quad (3)$$

Where, N_i is the total number of earthquakes recorded at that station. $HVSR_j$ represents the horizontal to the vertical spectral ratio of j^{th} station. The abscissa corresponding to the peak of the average H/V spectra ratio curve for a station is the predominant period at that station. Based on the predominant period at the station, a suitable site class is assigned by choosing an appropriate site classification scheme.

5.1. H/V spectral ratio from fast Fourier amplitude spectrum

The H/V spectral ratio of FFT was drawn to estimate the predominant period of the site

corresponding to the predominant peak of the H/V spectral ratio curve by following the procedure as stated above. Based on the predominant period of a station, the modified NEHRP site classification scheme (Harinarayan and Kumar, 2018a) given in Table 2 is selected to classify the sites into corresponding site classes.

Table 2. The site classification scheme used in Indian National Strong Motion Instrumentation Network's (NSMIN) recording stations as per modified NEHRP scheme (BSSC, 2004; Harinarayan and Kumar, 2018b, 2018a)

Site Class	General Description	V_{s30} *(m/s)*	Fundamental Frequency, $f_{0(Hz)}$	Fundamental Period, $T_{G(sec)}$
A	Hard rock	>1500	>12.71	<0.078
B	Rock	760 - 1500	6.35–12.70	0.078-0.157
C	Very dense soil and soft rock	360 - 760	3.05–6.35	0.157-0.328
D	Stiff soil	180 - 360	1.52–3.05	0.328-0.657
E	Soft soil	<180	<1.525	>0.657

5.2. H/V spectral ratio from response spectra

In this method, all steps given in the H/V spectral ratio curve procedure are followed. Instead of FFT, 5% damped response spectra are used at step 4, the predominant period from the H/V response spectral ratio curve is estimated (Macau et al., 2014; Perron et al., 2018). Site class definition, given in Table 3, categorizes sites as per the Japanese earthquake-resistant design code (JRA, 1980) and site classification scheme given in NEHRP site classes (BSSC, 2004). In this method, the predominant period of the site is one of the indexes for classification. When there are many earthquake records at a site, the average peak period from the H/V spectral ratio curve of 5% damped response spectra can be considered the site's predominant period. A site is classified as per the predominant period falls in the range of periods given in Table 3. The accuracy of this method is high while a large number of recordings are available at a site and reduces with the decrement of records at the site (Zhao et al., 2004). The shortcoming of this single index appears when H/V spectral curve has multiple peak periods. A similar approach was applied by Ghasemi et al. (2009) on the Iranian Strong Motion Network and Zhao et al. (2006) on the K-Net data set of Japan.

Table 3. The site classification scheme as per the Japan earthquake resistant design code (JRA, 1980; Zhao et al., 2006) and approximately corresponds to NEHRP site class (BSSC, 2004)

Site Class	Site Natural Period (*sec*)	Average shear wave velocity (m/s^2)	NEHRP Class
SC-I (Rock/Stiff Soil)	$T_G < 0.2s$	$V_s^{30} > 600$ m/s	A+B
SC-II (Hard Soil)	$0.2s \le T_G < 0.4s$	300m/s $< V_s^{30} \le 600$ m/s	C
SC-III (Medium Soil)	$0.4s \le T_G < 0.6s$	200m/s $< V_s^{30} \le 300$ m/s	D
SC-IV (Soft Soil)	$T_G \ge 0.6s$	$V_s^{30} \le 200$ m/s	E

5.3. H/V spectral ratio classification based on Zhao et al. (2006)

Zhao et al. (2006) used 5400 records from 122 earthquakes recorded at 874 K-Net strong-motion stations for site classification. They derived a geometric mean H/V spectral ratio of 5% damped response spectra, and standard deviations for each class is given in Fig. 5. The average H/V response spectral ratio amplitude and shape are remarkably different among four site classes, as shown in Fig. 5(a). It can be easily recognized from

Fig. 5(a) that curves of SC-I and SC-II show low amplitude in comparison to SC-III and SC-IV classes. These H/V spectral ratio curves show the resemblance and consistency to H/V spectral ratio curves proposed by Japan Road Association (JRA, 1980). The standard deviation at each site class curve is shown in Fig.5b. SC-III shows a slightly higher standard deviation than SC-I, SC-II, and SC-IV site classes. It might be due to this site class's relatively small number of stations. The entire standard deviation range is 0.25 to 0.55 for all site classes.

In this method, instead of using a single index (i.e., predominant period) for classification purposes, the peak period and shape of the H/V spectral ratio of all periods are used to increase the accuracy. This method is based on the probabilistic distribution of spectral shapes.

$$SI_k = \frac{2}{n}\sum_{i=1}^{n} F(-abs[\ln(\mu_i) - \ln(\bar{\mu}_{ki})]) \quad (4)$$

Where, *SI* is site index, k is site class number, n is total number of periods, $F()$ is normal cumulative distribution function, μ_i is mean H/V spectral ratio of site of interest for i^{th} period and $\bar{\mu}_{ki}$ is mean H/V spectral ratio for k^{th} site class averaged over all sites of the database for i^{th} period as shown in Fig. 5a.

SI is an index for site classification only. The standard deviation of each site class marginally enhances classification accuracy. For a particular period, *SI* equals unity only when the mean H/V spectral ratio for a site is equal to the mean H/V spectral ratio of that particular site class; otherwise, it is always less than one. For a particular site, *SI* is calculated for each site class, and the largest value of *SI* for that class is assigned as a class to that site. This method considers the amplitude and shape of the standard H/V spectral ratio curve in site classification.

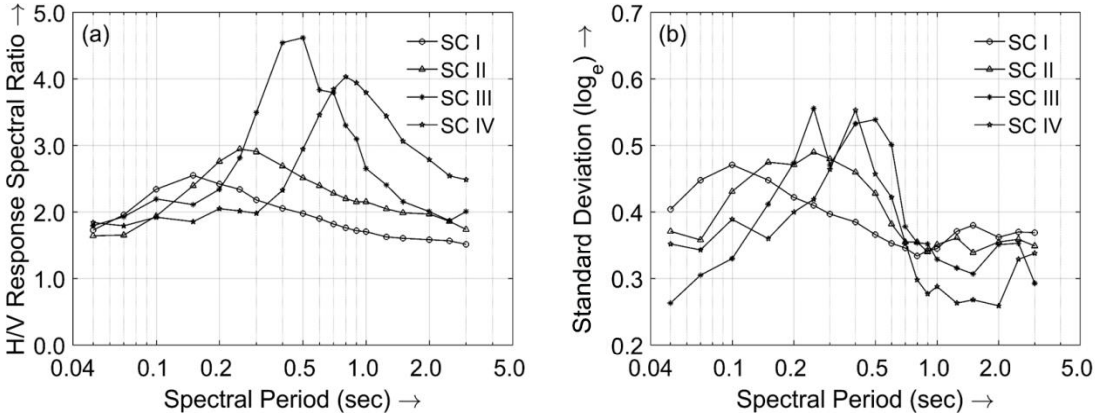

Figure 5. (a) Mean H/V response spectral ratio curve (b) Standard deviation corresponding to each class of K-Net dataset (Zhao et al., 2006)

5.4. H/V spectral ratio classification scheme based on Ghasemi et al. (2009)

Shape and amplitude of H/V spectral ratio curve of 5% damped response spectra for different site classes are used in section 5.3. By taking advantage of the shape and amplitude of the average H/V spectral ratio curve of standard response spectra of different site classes, Ghasemi et al. (2009) proposed a new method. According to this method, the site classification index can be designed as:

$$SI_k = 1 - 6\sum \frac{{d_i}^2}{n(n^2-1)} \quad (5.5)$$

Where, d_i is the difference between each rank of corresponding values of x_k and y, x_k is mean H/V spectral ratio curve of 5% damped

response spectra for k^{th} site class, y is mean H/V spectral ratio curve of 5% damped response spectra for site of interest, and n is total number of periods.

Proposed SI of this method is Spearman's rank correlation coefficient (Spearman, 2010). Statistically, it is a nonparametric (distribution-free) rank and measures association strength between two variables. In the perspective of site classification, it measures the correlation between average H/V spectral ratio curves for sites of interest and mean H/V spectral ratio curve of different site classes without making any assumptions about frequency/period distribution. The range of Spearman's correlation coefficient varies from -1 to 1. SI equals one indicates the perfect positive correlation between x and y. SI is calculated for each site class as calculated in section 5.3, and highest value of SI at a site is assigned as the respective site class of that site.

6. Smoothing of curves

Figure 6 represents three components (East-West, North-South, Up-Down) of the ground motion recorded at Adibadri station and their corresponding response spectra of magnitude 5.5 Rudraprayag earthquake, which occurred on Dec. 6, 2017. The depth of this earthquake was 30 Km. Epicenter of this earthquake from Adibadri station was 29.4 Km. A 5% damped response spectra of all three components are created to draw this station's H/V response spectral ratio (Fig. 7). Konno - Ohmachi smoothing is applied (Konno and Ohmachi, 1998). A smoothed H/V spectral ratio curve is shown in Fig. 7. The apparent peak from the curve can be easily identified from the figure and similarly its corresponding spectral period.

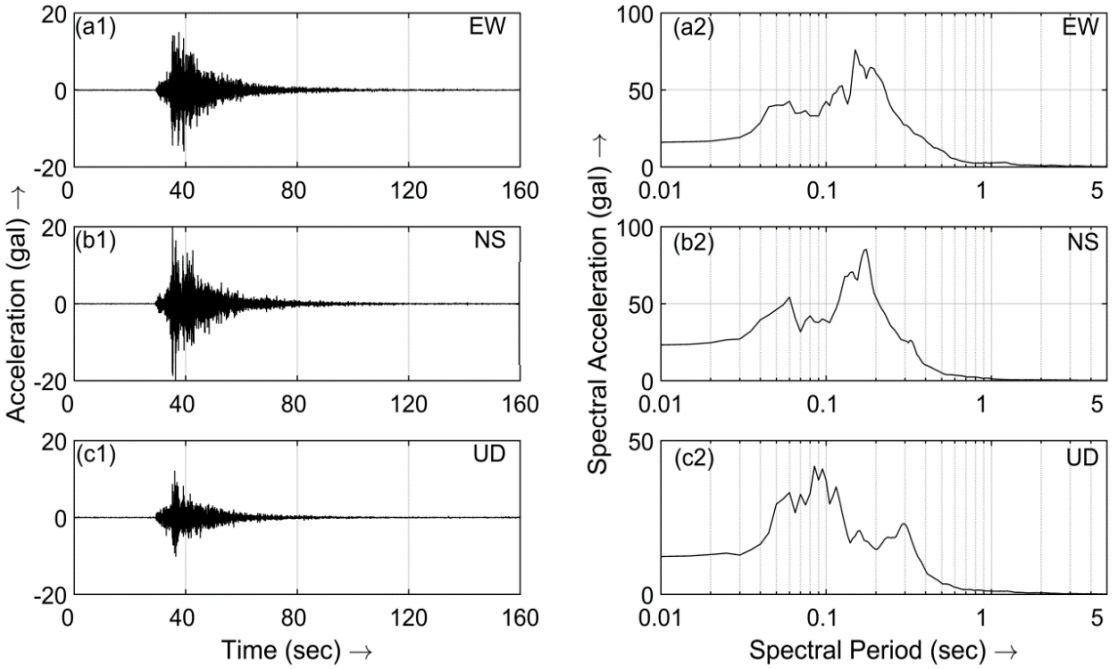

Figure 6. Acceleration and their corresponding response spectra of EW, NS and UD components at Adribadri station of the earthquake of Mw-5.5, triggered on Dec. 6, 2017, in Rudraprayag, Uttarakhand

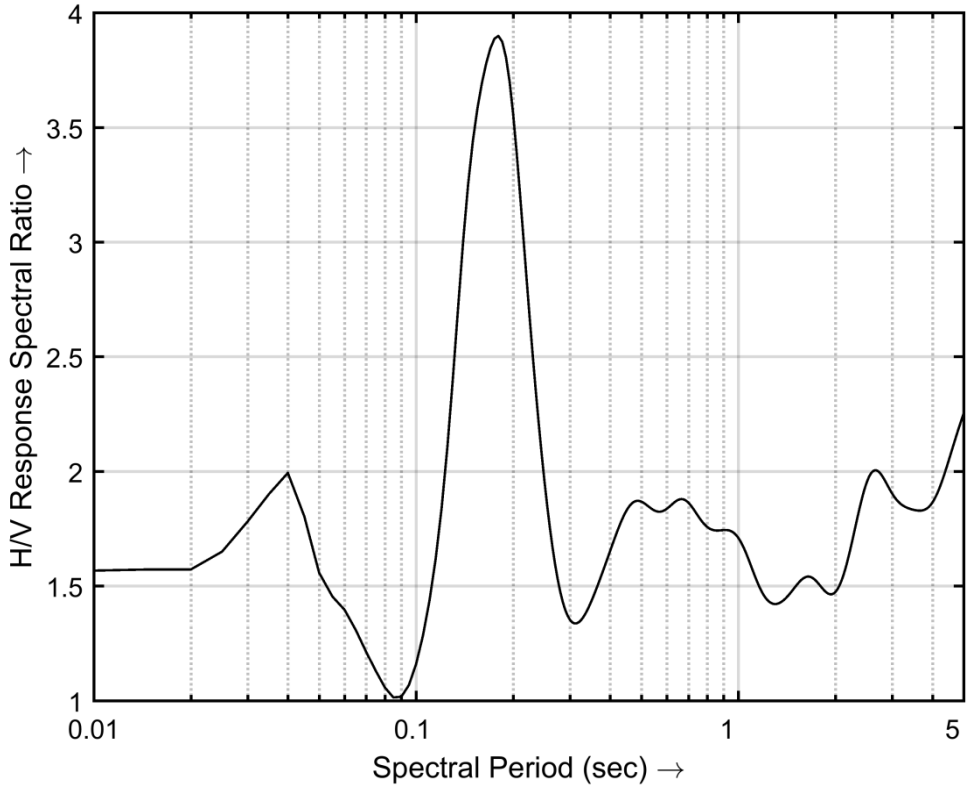

Figure 7. The H/V response spectral ratio curve was created using the records from Adibadri station of the earthquake of Mw 5.5 triggered on Dec. 6, 2017, in Rudraprayag, Uttarakhand. The peak is easily recognizable from this H/V response spectral ratio curve, and thus its corresponding period

7. Effect of depth, distance and magnitude on H/V spectral ratio curves

Classification of the site based on the H/V spectral ratio is a stable method. The created 5% damped response spectra show that it depends on the earthquake's magnitude, distance, and depth, but their ratios are almost independent of magnitude, distance, and depth (Wen et al., 2011; Yamazaki and Ansary, 1997). This has also been researched by Zhao et al. (2006) using the K-Net dataset of the Japan Meteorological Agency. Dataset used in this study consists of the near field to far-field records, and effect of magnitude, distance and depth on the H/V spectral ratio curve has shown on the four stations classified into four classes. Figure 8(a) is the H/V spectral ratio curve of the earthquake records of magnitude ranging from 3.8 to 6.2, depth 10 to 190 Km, and epicentral distance from 29 to 1199 Km. Fig. 8b is a H/V spectral ratio curve of magnitude ranging from 4.5 to 6.9, epicentral distance 58 to 667 Km, and depth 10 to 33 Km. Figure 8c is a H/V spectral ratio curve of magnitude ranging from 4.3 to 6.0, epicentral distance 160 to 609 Km and depth 10 to 33 Km. Figure 8d is a H/V spectral ratio curve of magnitude ranging from 3.5 to 6.2, epicentral distance 22 to 1191 Km, and depth 10 to 190 Km. It is evident that the magnitude, epicentral distance and depth have an almost negligible effect on average H/V spectral ratio curves.

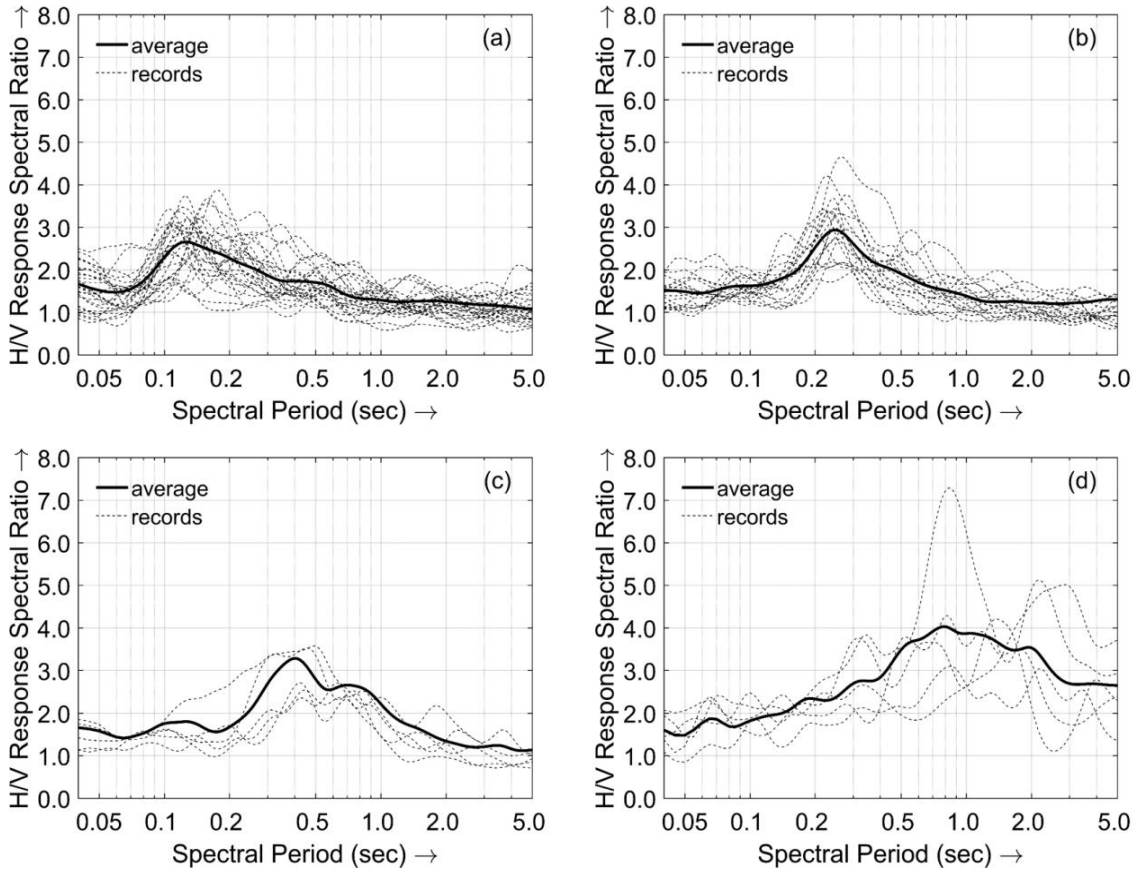

Figure 8. (a) Average H/V spectral ratio curve of class-B, (b) Average H/V spectral ratio curve of class-C, (c) Average H/V spectral ratio curve of class-D, (d) Average H/V spectral ratio curve of class-E

8. Effect of damping ratio

Change in damping ratio does not significantly affect the predominant period of the ground obtained from the H/V spectral ratio curve. It is demonstrated with an example. Figure 9a is the H/V spectral ratio curve of Fourier amplitude spectra (FAS) of the ADIB station and the estimated period is 0.181 seconds with a standard deviation of 0.00907 seconds. Figure 9b is the H/V spectral ratio curve of 0% damped response spectra of horizontal and vertical components of the records at the same station. It can be observed that the H/V spectra ratio curve from FAS and 0% damped response spectra are almost similar. The estimated spectral period from the H/V spectral ratio curve of 0% damped response spectra is 0.18 seconds with a standard deviation of 0.009 seconds. A similar spectral period is found in the H/V spectral ratio of 5% and 10% damped response spectra curves, as shown in Figs. 9 (c, d). It is observed that in long period motions, the peak value of total acceleration may occur during later arrivals of surface waves, and in short period motions, the peak value may occur before the time of S-wave arrival. The vertical component of ground motion occasionally shows the peak value of total acceleration before the time of S-wave arrival. The 5% damped response spectra of acceleration show a similar shape to the FAS except at brief periods, and sharp peaks are

not present in the response spectra as usually occurs in FAS. The sharp peaks current in the FAS sometimes lead to considerable variability in the average H/V spectral ratio. Another advantage of 5% damped response spectra is smoothing the curve (Zhao et al., 2006). A high percentage of damped spectra does not significantly affect the spectral period corresponding to the peak of the H/V spectral curve of response spectra. Therefore, 5% damped response spectra are used in this study.

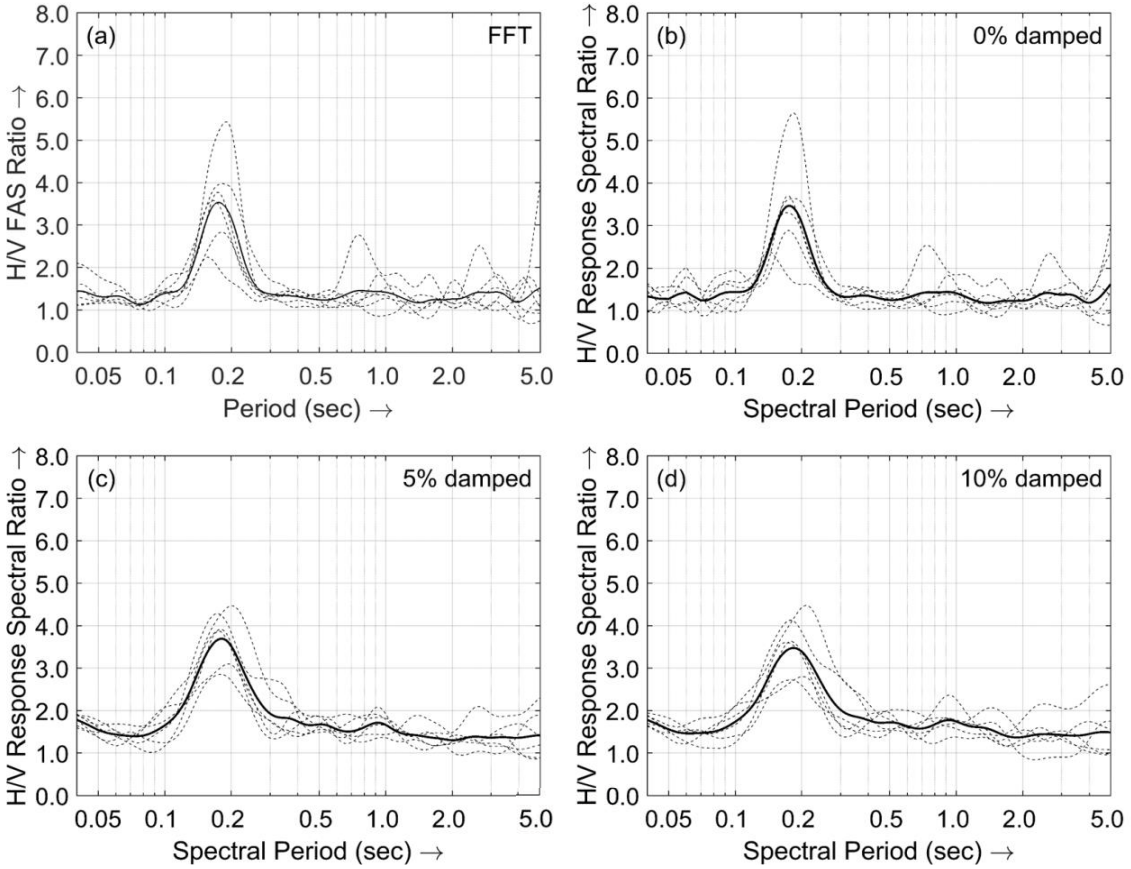

Figure 9. At Adibadri site (a). H/V spectral response curve from FAS (b). H/V response spectral ratio curve from 0% damped response spectra (c). H/V response spectral ratio curve from 5% damped response spectra (d). H/V response spectral ratio curve from 10% damped response spectra

9. Discrepancies in H/V spectral ratio curve

The classification methods stated in section 5.3 and 5.4 have been applied in many countries or regions, namely Japan (Zhao et al., 2006), Iran (Ghasemi et al., 2009), Taiwan (Lee et al., 2001), China (Ji et al., 2017; Wen et al., 2011) and Italy (Alessandro et al., 2012), etc. They have used standard curves and applied methods to calculate site indexes for classification. The high success rate of each classification is always not possible for all the regions. Site response at different stations is highly affected by non-linear, complex, and heterogeneous subsoil layers. The joggling phenomena at the head and tail of response spectra were first explained by

Wen et al. (2011) and developed entropy weight theory to overcome this problem to some extent. At many stations, it has been observed that the H/V spectral ratio curves are flat with no predominant peak; therefore, the predominant period is indeterminable so does their classification. At some sites, the H/V spectral ratio curve shows multiple peaks; hence predominant period can not be defined. Therefore, those sites were excluded where these kinds of discrepancies were found.

10. Results

The total records from regional (i.e., serial numbers 1 to 32 in Table 1) and far-field (i.e., serial numbers 33 to 38 in Table 1) are 465 and 130, respectively. SNR and PGA criteria are applied over the seismic records to select suitable quality records. It was found that a total of 335 records of 52 stations qualified for these conditions. First of all, Nakamura's (1989) methodology was applied to the strong ground motion records in method-1. The H/V spectral ratio curves were created for all the stations. Predominant period and amplitude corresponding to the peak in the curve is given in Table 4. In the second method, 5% damped response spectra of three components of all the records were created, then H/V response spectra were used. The amplitude and period corresponding to the peak of the H/V response spectra curve were estimated and given in Table 4. In method-1, the site classification scheme shown in Table -2 is applied. In method-2, the site classification scheme provided in Table 3 (JRA, 1980) is used. The site classification index was calculated for all the stations as per method 3 (Zhao et al., 2006), and the resultant classification is given in Table 4. Another site classification index based on Spearman's rank correlation function for all the stations was calculated as per method-4 (Ghasemi et al., 2009), and the corresponding classification is given in Table 4.

Table 2. The site classification scheme used in Indian National Strong Motion Instrumentation Network's (NSMIN) recording stations as per modified NEHRP scheme (BSSC, 2004; Harinarayan and Kumar, 2018b, 2018a)

Site Class	General Description	V_{s30} *(m/s)*	Fundamental Frequency, $f_{0(Hz)}$	Fundamental Period, $T_{G(sec)}$
A	Hard rock	>1500	>12.71	<0.078
B	Rock	760-1500	6.35-12.70	0.078-0.157
C	Very dense soil and soft rock	360-760	3.05-6.35	0.157-0.328
D	Stiff soil	180-360	1.52-3.05	0.328-0.657
E	Soft soil	<180	<1.525	>0.657

Table 3. The site classification scheme as per the Japan earthquake resistant design code (JRA, 1980; Zhao et al., 2006) and approximately corresponds to NEHRP site class (BSSC, 2004)

Site Class	Site Natural Period (*sec*)	Average shear wave velocity (m/s^2)	NEHRP Class
SC-I (Rock/Stiff Soil)	$T_G < 0.2s$	$V_s^{30} > 600$ m/s	A+B
SC-II (Hard Soil)	$0.2s \le T_G < 0.4s$	300m/s $< V_s^{30} \le 600$ m/s	C
SC-III (Medium Soil)	$0.4s \le T_G < 0.6s$	200m/s $< V_s^{30} \le 300$ m/s	D
SC-IV (Soft Soil)	$T_G \ge 0.6s$	$V_s^{30} \le 200$ m/s	E

Table 4. List of the sites which are classified into site classes based on modified NEHRP scheme, JRA site classification schemes and method -3, -4

a	b	c	d	E	f	g	H	i	j	k	l	m	n	o
1	Adibadri	ADIB	3.54	0.45	0.18	0.01	C	3.70	0.31	0.18	0.01	B	B	B
2	Augustmuni	AGMS	1.77	0.21	0.09	0.00	B	1.91	0.18	0.15	0.01	B	B	B
3	Bhiri	BHIB	1.55	0.16	0.20	0.01	C	2.07	0.18	0.17	0.01	B	B	B
4	Bhilangna	BHLS	3.07	0.47	0.24	0.00	C	2.25	0.24	0.25	0.01	C	B	C
5	Barkot	BKTS	3.15	0.55	0.39	0.02	D	4.63	0.73	0.38	0.02	C	D	D
6	Chandrapuri	CDPB	5.17	0.81	0.21	0.01	C	4.28	0.55	0.20	0.01	B	C	C
7	Chamba B	CMBB	2.07	0.26	0.13	0.01	B	2.54	0.18	0.13	0.01	B	B	B
8	Chamba S	CMBS	2.30	0.30	0.30	0.02	C	3.03	0.60	0.29	0.02	C	C	C
9	Chamiyala	CMLB	3.58	0.57	0.12	0.01	B	4.34	0.32	0.12	0.01	B	C	B
10	Chhinka	CNKB	4.37	0.72	0.13	0.01	B	4.16	0.41	0.16	0.01	B	C	B
11	Chinyalisour	CYSB	2.23	0.34	0.09	0.01	B	2.73	0.16	0.14	0.01	B	B	B
12	Dhari	DHRI	2.07	0.29	0.81	0.00	E	1.96	0.34	0.88	0.04	E	B	E
13	Dhanaulti	DLTB	4.64	0.88	0.28	0.00	C	2.50	0.28	0.22	0.01	C	B	B
14	Dhauntri	DNTB	2.73	0.48	0.09	0.01	B	3.17	0.32	0.08	0.00	B	B	E
15	Durgadhar	DRDB	1.99	0.32	0.21	0.01	C	2.52	0.34	0.36	0.02	C	B	C
16	Dunda	DUNB	2.60	0.36	0.25	0.01	C	3.25	0.40	0.23	0.01	C	B	B
17	Deval	DVLS	3.48	0.45	0.46	0.02	D	2.92	0.51	0.43	0.02	D	C	D
18	Devprayag	DVPS	2.36	0.36	0.21	0.01	C	3.14	0.39	0.23	0.01	C	B	B
19	Gaza	GAZB	2.14	0.28	0.26	0.01	C	2.56	0.39	0.26	0.01	C	B	C
20	Gaucher	GCRB	1.80	0.19	0.58	0.03	D	2.07	0.28	0.61	0.03	E	B	D
21	Ghurdauri	GDRB	2.22	0.31	0.18	0.00	C	2.03	0.13	0.17	0.01	B	B	C
22	Gwaldom	GLMB	2.26	0.35	0.12	0.01	B	2.48	0.28	0.12	0.01	B	B	B
23	Gholteer	GLTB	2.44	0.35	0.40	0.02	D	2.59	0.37	0.38	0.02	C	B	C
24	Ghansali	GNSB	3.42	0.49	0.12	0.01	B	3.73	0.38	0.12	0.01	B	B	B
25	Gopeshwar B	GOPB	2.59	0.41	0.78	0.00	E	2.55	0.41	0.74	0.04	E	B	D
26	Gopeshwar S	GOPS	3.58	0.46	0.73	0.04	E	3.87	0.61	0.64	0.03	E	C	D
27	Gairsain	GRSB	2.01	0.25	0.19	0.01	C	2.05	0.28	0.26	0.01	C	B	C
28	Gyanshu	GYNB	2.44	0.33	0.18	0.01	C	3.24	0.41	0.18	0.01	B	B	B
29	Jhakhnidhar	JKDB	1.57	0.18	0.24	0.01	C	2.85	0.31	0.22	0.01	C	B	B
30	Jakholi	JKLS	3.72	0.54	0.24	0.01	C	3.17	0.36	0.22	0.01	C	C	C
31	Jamnikhal	JMKB	2.55	0.35	0.16	0.01	C	2.63	0.20	0.16	0.01	B	B	B
32	Joshimath	JMTB	1.97	0.20	0.65	0.03	D	2.06	0.31	0.68	0.03	E	B	D
33	Khankra	KNKB	3.41	0.54	0.11	0.01	B	3.89	0.36	0.10	0.01	B	B	B
34	Kanatal	KNTB	1.73	0.22	0.31	0.00	C	2.09	0.21	0.30	0.02	C	B	C
35	Khirsu	KRSB	2.69	0.43	0.12	0.01	B	3.29	0.46	0.11	0.01	B	B	B
36	Langasu	LNGB	3.16	0.58	0.15	0.01	B	3.05	0.34	0.12	0.01	B	B	B
37	Mahidanda	MHDB	2.31	0.26	0.29	0.01	C	2.35	0.30	0.28	0.01	C	B	B
38	Maneri	MNRB	3.51	0.57	0.14	0.00	B	2.55	0.26	0.13	0.01	B	B	B
39	Matli	MTLB	3.15	0.60	0.12	0.01	B	2.89	0.32	0.12	0.01	B	B	B
40	Nandprayag	NNPB	2.69	0.34	0.37	0.02	D	2.77	0.30	0.35	0.02	C	B	C
41	Nauti	NTYB	1.78	0.18	0.23	0.01	C	2.11	0.19	0.21	0.01	C	B	B
42	Pipalkoti	PLKB	2.71	0.44	0.24	0.01	C	3.01	0.46	0.33	0.02	C	B	C
43	Pauri	PORS	3.62	0.69	0.12	0.01	B	5.79	0.68	0.11	0.01	B	B	B
44	Purola	PRLS	3.85	0.59	0.23	0.01	C	4.93	0.57	0.20	0.01	C	B	B
45	Paithani	PTHB	2.77	0.37	0.22	0.01	C	2.74	0.33	0.20	0.01	C	B	B
46	Ranichauri	RCRB	2.57	0.27	0.45	0.02	D	2.72	0.41	0.30	0.02	C	B	D
47	Srikot	SKTB	3.64	0.45	0.18	0.01	C	3.76	0.34	0.17	0.01	B	B	C
48	Simli	SMLB	2.46	0.35	0.11	0.01	B	2.52	0.22	0.11	0.01	B	B	B
49	Srinagar	SRNS	2.17	0.32	0.14	0.01	B	2.31	0.25	0.14	0.01	B	B	B
50	Thatyur	THTB	3.36	0.51	0.12	0.01	B	4.53	0.40	0.12	0.01	B	B	B
51	Tharali	TRLS	1.74	0.38	0.15	0.01	B	2.11	0.25	0.15	0.01	B	B	B
52	Utterkashi	UTKS	2.56	0.40	0.12	0.00	B	3.25	0.32	0.12	0.01	B	B	B

←*Note:* (a) Serial number, (b) Name of station, (c) Short Code of the stations, (d) Amplitude at the peak of the H/V FAS ratio, (e) Error of Amplitude at the peak of the H/V FAS ratio, (f) Period at the peak of H/V FAS ratio, (g) Error in the period of H/V FAS ratio, (h) classification as per JRA scheme, (i) Amplitude at the peak of H/V response spectra, (j) Error in Amplitude at the peak of H/V response spectra, (k) Spectral Period at the peak of H/V response spectra, (l) Error in spectral period at the peak of H/V response spectra, (m) Classification based on method-2, (n) Classification based on the site classification index of method-3, (o) Classification based on the site classification index of method-4

11. Discussions

As given in Table 4, sites are classified using the estimated period from the H/V spectral ratio of FAS and H/V spectral ratio of 5% damped response spectra using the classification schemes given in Tables 2 and 3, respectively. Site classification of a few sites in Table 4 is also classified by many researchers using different approaches. Classification of the six stations, namely Ghansali, Dhanaulti, Joshimath, Pauri, Uttarkashi and Barkot, was first carried out as part of Indian NSMIN stations of the Garhwal region by Mittal et al. (2012). These stations were classified by considering the lithology of the region (Mittal et al., 2012) and by applying modified Borcherdt's classification scheme (Borcherdt, 1994). At these locations, accelerometers of the EEW System have also been installed. Further, Harinarayan and Kumar (2018b) used the records of the earthquakes from the Indian NSMIN stations dataset viz., Program for Excellence in Strong Motion Studies (PESMOS) to classify these sites by applying the H/V spectral ratio curve technique. These earthquakes were triggered from Dec. 2005 to Dec. 2009, and their magnitudes range from 3.5 to 6.4. As Mittal et al. (2012) used the site lithology and Harinarayan and Kumar (2018b) used the strong ground motion data of the triggered earthquake at these stations for classification purposes; therefore, Pandey (2018) carried out field tests for classification. These field tests are MASW using Soil Spy Rosina and records of microtremors from Tromino. The joint inversion technique using Grilla software was applied on H/V spectral response of ambient vibrations and MASW to estimate the site's shear wave velocity profile (Pandey, 2018). Then, the sites were classified based on estimated V_{s30} using the NEHRP scheme. Dhanaulti site was classified in site class-B by Mittal et al. (2012) after examining the lithology of the site (Borcherdt, 1994), Harinarayan and Kumar (2018b) used strong ground motion records and classified this site in class-C using a modified NEHRP scheme, Pandey (2018) classified this site based on V_{s30} in class-C using NEHRP scheme. The present study is classified in class-C using both modified NEHRP and JRA schemes. Ghanshali site is classified in class-A after examining the lithology of the site (Mittal et al., 2012), Harinarayan and Kumar (2018b) classified this site in class-C using NEHRP scheme, Pandey (2018) classified this site in class-C using NEHRP scheme, and predominant period of this site estimated after applying Generalized inversion (GINV) method also falls in class-C of JRA scheme (Sharma et al., 2014). In the present study, this site is classified in class-B using modified NEHRP and JRA schemes. Pauri site is classified in class-A by Mittal et al. (2012) considering lithology of the site and in class-B by Harinarayan and Kumar (2018b), Sharma et al. (2014), and Pandey

(2018) using NEHRP scheme. In the present study, it is classified in site class-B. Joshimath site is classified in class-E by Harinarayan and Kumar (2018b), and in the present study, this site is classified in class-D using modified NEHRP scheme and in class-E using JRA scheme. Uttarkashi site is classified in class-B by Pandey (2018) using Borcherdt's (1994) scheme, and in the present study, it is also classified in class-B using both JRA and modified NEHRP scheme. Barkot site is classified in class-B by Mittal et al. (2012) and Harinarayan and Kumar (2018b) using Borcherdt (1994) scheme, in class-C by Pandey (2018), Harinarayan and Kumar (2018b), Sharma et al. (2014) using NEHRP classification scheme. In the present study, this site is classified in class-D using a modified NEHRP scheme and in class-C using the JRA scheme. A similitude of the classification of these few sites with the classification done in the previous studies is also shown in Table 5.

Table 5. Classification of a few sites that were classified in the erstwhile studies with the present classification

Station Name	Short Code	Mittal et al. (2012)	Harinarayan and Kumar (2018b)	Pandey et al. (2018)	Sharma et al. (2014)	Present Study				
		Borcherdt (1994) scheme	NEHRP (BSSC, 2003) scheme	NEHRP (BSSC, 2003) scheme	JRA (1980) scheme	NEHRP (BSSC, 2003) scheme	JRA (1980) scheme	Zhao et al. (2006)	Ghasemi et al. (2009)	Final Class
Barkot	BKTS	B	C	C	C	D	C	D	D	D
Dhanaulti	DLTB	B	C	C	-	C	C	B	B	C
Ghanshali	GNSB	A	C	C	C	B	B	B	B	B
Joshimath	JMTB	-	E	-	-	D	E	B	D	D
Pauri	PORS	A	B	B	B	B	B	B	B	B
Uttarkashi	UTKS	-	-	B	-	B	B	B	B	B

The predominant period of all 52 sites is given in columns (f) and (k) from the H/V spectral ratio curve of FAS and 5% damped response spectra. These sites are classified into different classes using modified NEHRP and JRA schemes. Method-1 used the predominant period of sites measured from the H/V spectral ratio of FAS, and sites are classified as per the modified NEHRP scheme. In method-2, dominant periods are measured from the H/V spectral ratio curve of 5% damped response spectra, and sites are classified according to the JRA scheme. In Method-3, a site index has been used. In method-4, Spearmans's rank correlation coefficient as site index has been used. Figure 10 shows the bar chart of the number of sites classified by methods - 1, -2, -3, and -4.

The predominant period of sites is compared with the range of periods given in Tables 2 and 3 for classification. To know the success rate of a method, its classified sites need to be compared with the same sites classified by method-2.Method-2 is manual classification, and it is considered that manual classification is vital to get the best results. After analyzing all 52 sites, the success rate of method-3 (Zhao et al., 2006) for SC-B is 88.46%, SC-C is 10%, no site is classified in class-D, -E, and the overall success rate is 48.07.6%. The success rate for method-4 (Ghasemi et al., 2009) for SC-B is 84.61%, SC-C is 50.00%, SC-D is 100%, SC-E is 20%, and the overall success rate of this method is 65.38%. The success rate of method-1 for SC-

B is 73.07%, SC-C is 80.00%, SC-D is 100%, SC-E is 60%, and the overall success rate is 75.00%. Figure 11 shows the comparative success rate of these methods.

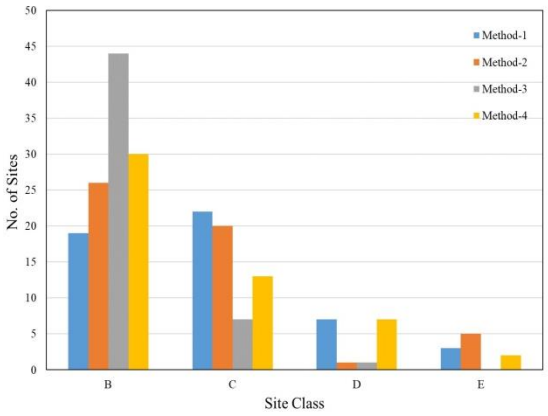

Figure 10. Classification of sites

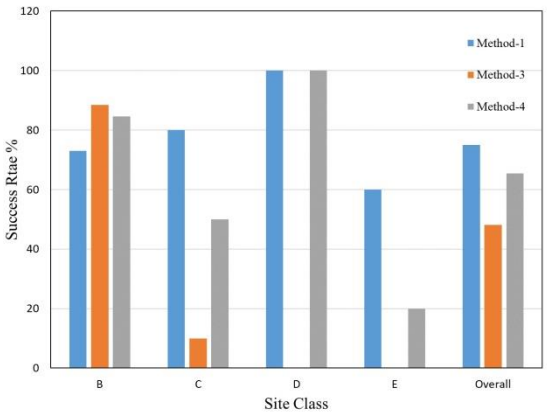

Figure 11. The success rate of method-1, -3, and -4 with respect to method-2

12. Final site classification

Site classification schemes adopted in this study are modified NEHRP (Harinarayan and Kumar, 2018a) and JRA schemes (Japan Road Association, 2002). JRA scheme classifies the sites into four classes, namely I, II, III, and IV, as given in Table 3, while NEHRP based scheme classifies sites into five classes, namely A, B, C, D, and E, as given in Table 2. In the JRA scheme, sites A and B are merged into one site class -B. Site class-E represents a potentially liquefiable site while site classes -B, -C, -D represent rock/stiff soils, hard soils, and medium soil, respectively. The modified NEHRP scheme based on Harinarayan and Kumar, (2018a) classification, classifies sites into five classes -A, -B, -C, -D, -E. This study classified no site in class-A as per the modified NEHRP scheme. Class-A and -B of NEHRP are merged into one class (i.e., SC-I) in the JRA scheme. Therefore, in this study, SC-A is not prominent, and thus, this class is also merged into SC-I of the JRA scheme. Instead of using roman numeric in site class nomenclature, alphabetical order is used to categorize sites (i.e., SC-I, -II, -III, -IV of JRA scheme are used as SC - B, -C, -D, -E) in this study. The final classification of all 52 stations is given in Table 6.

By considering the average H/V spectral ratio curve obtained from similar site class, the overall H/V curve is developed for all the site classes -B, -C, -D, and -E. Figure 12 represents the average H/V curve for site classes-B, -C, -D, and -E with the predominant period 0.13, 0.25, 0.4 and 0.78 seconds, respectively. Site class-B represents rock/stiff soil; therefore, the predominant period is low in comparison to site class-C, -D, and -E.

By analyzing the shape and predominant period in H/V spectral ratio curves of FAS and 5% damped response spectra, 52 sites are classified by taking advantage of the site classification index of Zhao et al. (2006) and Ghasemi et al. (2009) methods. Final site classes are assigned comparing assigned classes from all four methods. The highest

frequency of assigned class at a site by all the four methods is voted for the final classification of that site. The re-classification of sites is given in Table 6. The table shows that out of 52 stations, 23 sites are classified in class-B, 21 sites in class-C, 5 sites in class-D, and 3 sites in class-E.

The estimated predominant periods by H/V spectral ratio curve of 5% damped response spectra at the locations of sensors of EEW System for Uttarakhand are plotted on the map, and the corresponding contouring of the predominant period in the instrumented region is shown in Fig. 13.

Table 6. Final classification of 52 sites

S.N.	Code	SC	S.N.	Code	SC	S.N.	Code	SC	S.N.	Code	SC
1	ADIB	B	14	DNTB	B	27	GRSB	C	40	NNPB	C
2	AGMS	B	15	DRDB	C	28	GYNB	B	41	NTYB	C
3	BHIB	B	16	DUNB	C	29	JKDB	C	42	PLKB	C
4	BHLS	C	17	DVLS	D	30	JKLS	C	43	PORS	B
5	BKTS	D	18	DVPS	C	31	JMKB	B	44	PRLS	C
6	CDPB	C	19	GAZB	C	32	JMTB	D	45	PTHB	C
7	CMBB	B	20	GCRB	D	33	KNKB	B	46	RCRB	D
8	CMBS	C	21	GDRB	C	34	KNTB	C	47	SKTB	C
9	CMLB	B	22	GLMB	B	35	KRSB	B	48	SMLB	B
10	CNKB	B	23	GLTB	C	36	LNGB	B	49	SRNS	B
11	CYSB	B	24	GNSB	B	37	MHDB	C	50	THTB	B
12	DHRI	E	25	GOPB	E	38	MNRB	B	51	TRLS	B
13	DLTB	C	26	GOPS	E	39	MTLB	B	52	UTKS	B

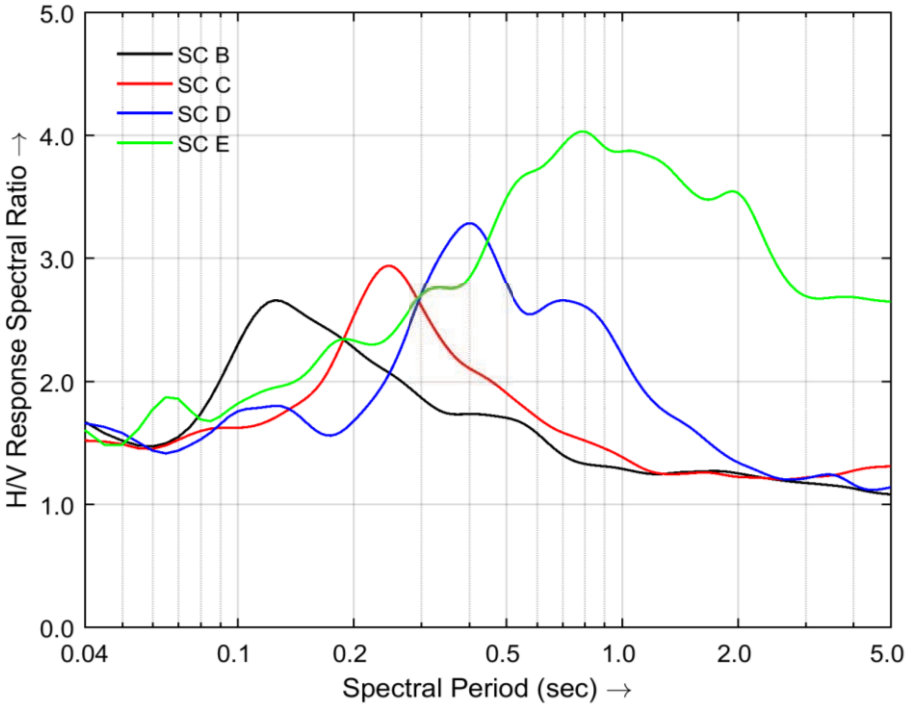

Figure 12. Average H/V response spectral ratio curves for site classes -B, -C, -D, and -E were obtained in the present study.

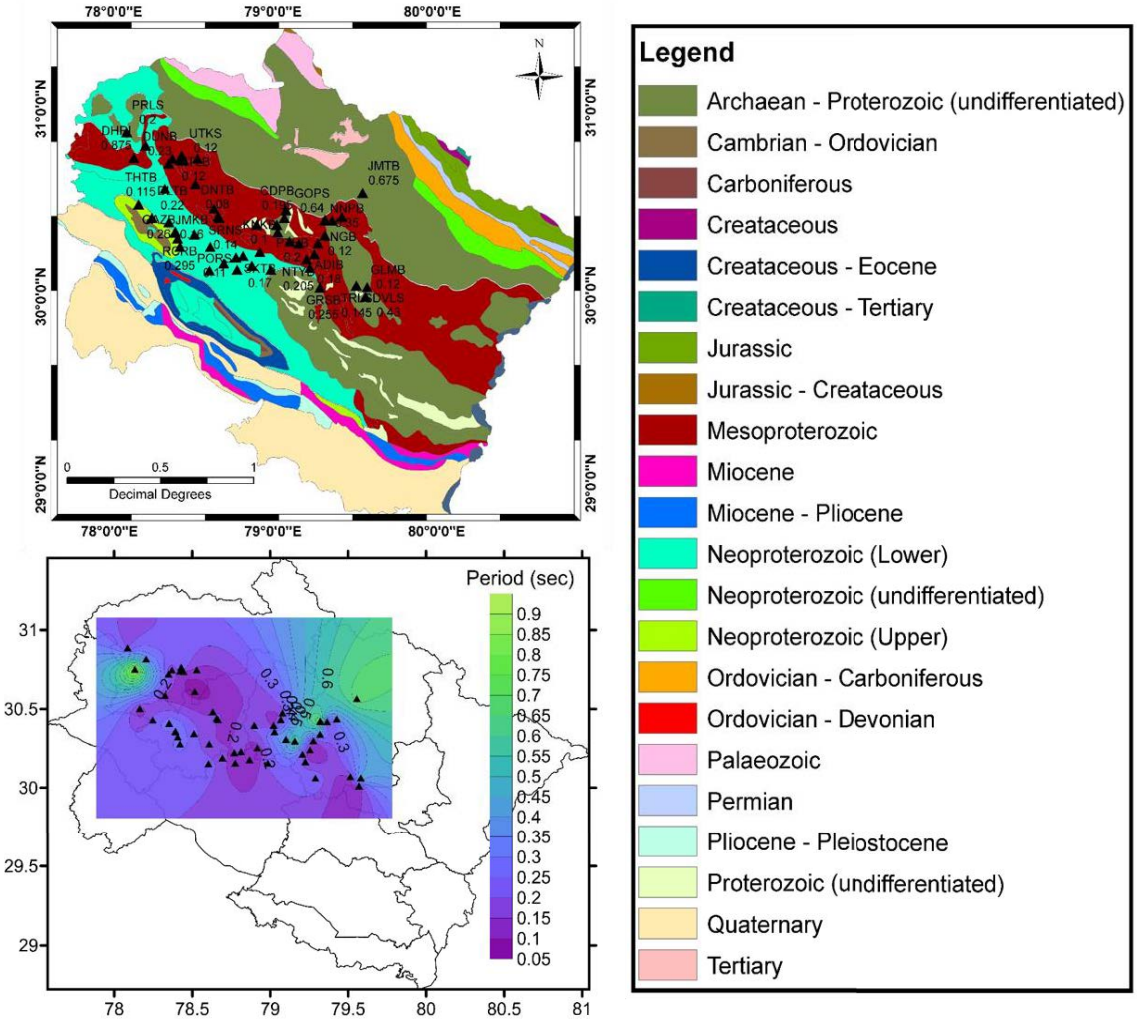

Figure 13. (a) shows the sites with the period estimated by H/V spectral ratio. (b) shows the contour of the period in the Garhwal region

13. Validation

The average H/V curves obtained from the 5% damped response spectra show an excellent match to the H/V spectral ratio curve of SC-I, SC-II, SC-III, and SC-IV proposed by Zhao et al. (2006) as shown in Fig. 14 a-d. The SC-I of Zhao et al. (2006) corresponds to NEHRP SC-A and SC-B. The SC-II, SC-III, and SC-IV of Zhao et al. (2006) correspond to NEHRP site class-C, -D, and -E, respectively. It can be observed from Fig. 14 a-d that the peak and shape of the H/V response spectra curve obtained from the intermediate site classes of -B, -C, -E match well with the site classes -I, -II, -IV as given by Zhao et al. (2006). However, the predominant period of SC-III (Zhao et al., 2006) is higher than the site class-D of the present study. It might be due to the low magnitude records used in the present study. It must be noted here that the current work primarily focuses on the shape and period of the ground corresponding to the peak of the H/V response spectra curve. However, a different amplitude value at the predominant peak can be observed. This difference in

amplitude at the predominant peak might be because, in the present study, around 73% of data corresponds to earthquakes with magnitudes less than five. Thus, their low peak ground acceleration records. However, H/V response spectra ratio curves proposed by Zhao et al. (2006) were prepared using earthquakes with magnitudes greater than five. Thus, in the present study, obtained curve amplitude may vary but shape and period range will be consistent with H/V response spectra ratio curves proposed by Zhao et al. (2006).

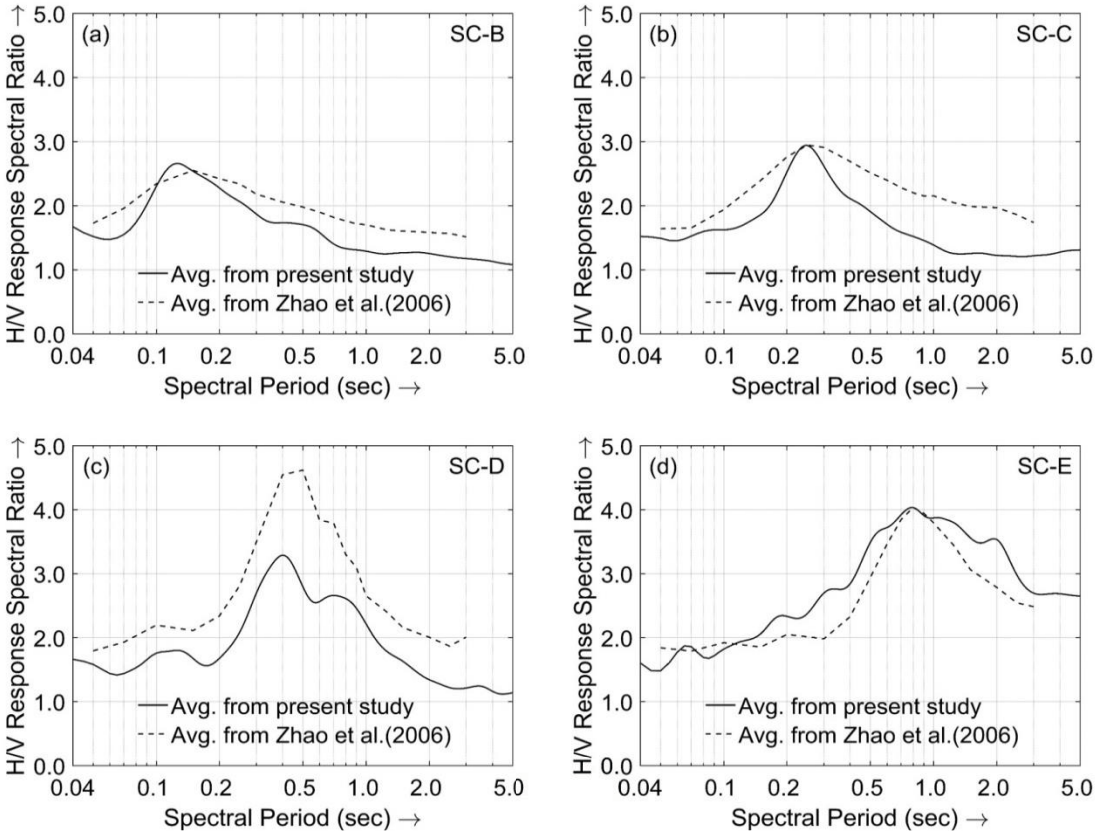

Figure 14. Comparison of obtained response spectra for the Uttarakhand region to the response spectra from Zhao et al. (2006)

14. Conclusions

The seismic network array of the EEW System for Uttarakhand in the Garhwal region comprises 84 sensors installed in the hilly part of the province. The strong ground motion records of the earthquakes were recorded on the server installed in the EEW System Laboratory, IIT Roorkee. In the present study, earthquake records from 2015 to 2019 are analyzed and used for classification purposes. We draw our conclusions as below:

(1) Two qualification criteria, namely SNR and PGA, are applied to the strong ground motion records of the earthquakes. After preprocessing of the data, records of only 52 stations qualified the applied constraints required to choose good quality data.

(2) The H/V spectral ratio curves of all the stations are created by FAS and 5% damped response spectra. The predominant period from the ratio curves is estimated for each site.

(3) Effects of earthquakes' depth, distance, and magnitude on H/V spectral ratio curves are discussed and analyzed. It was found that these factors do not affect the predominant period in the H/V spectral ratio curve of the site.

(4) Also, the effect of change in damping ratio percentage in the response spectra method is discussed, and it was observed that the change in damping ratio percentage does not affect the predominant period in the H/V spectral ratio curves.

(5) Four methods have been used for classification. In the first method, the predominant period is estimated by the H/V spectral ratio curve of FAS. In the second method, the predominant period is estimated by the H/V spectral ratio curve of 5% damped response spectra of the records. The third method is based on an empirical approach, and a site index for classification uses a cumulative distribution function (Zhao et al., 2006). The fourth method is based on Spearman's rank correlation coefficient and uses a site index for classification (Ghasemi et al., 2009). Final site class has been assigned comparing assigned classes from all four methods. The highest rate of recurrence of an assigned class at a site by all the four methods is voted for the final classification of that site. Two classification schemes, namely the modified NEHRP scheme (Harinarayan and Kumar, 2018a) in first method and JRA (1980) scheme in second method, have been used to classify the sites. In the present study, the H/V spectral ratio curve for each site class matches well with the standard H/V spectral ratio curves proposed by Zhao et al. (2006).

Acknowledgments

The authors are thankful to Dr. B.K. Gairola, Dr. V.P. Dimri, Prof. Ajay Gairola, Prof. M.L. Sharma, Prof. R.S. Jakka, Dr. Himanshu Mittal, Mr. Bhanu Pratap Chamoli, Mr. Govind Rathor, Dr. Rajiv Sachdeva for their suggestions and support in the EEW System laboratory. The authors are thankful to the Ministry of Earth Science for providing the fund for the project entitled 'Development of Earthquake Early Warning System for Northern India' as a pilot project and also thankful to the USDMA, Dehradun, Government of Uttarakhand for providing the fund to run the 'EEW System for Uttarakhand' as a full-fledged operational project.

References

Alessandro C. Di, Bonilla L.F., Boore D.M., Rovelli A., Scotti O., 2012. Predominant-period site classification for response spectra prediction equations in Italy. Bull. Seismol. Soc. Am., 102, 680-695. https://doi.org/10.1785/0120110084.

Borcherdt R.D., 1970. Effect of Local Geology on Ground Motion near San Francisco Bay*. Bull. Seismol. Soc. Am., 60, 29-61.

BSSC, 2004. NEHRP Recommended Provisions for Seismic Regulations for New Buildings and other Structures (FEMA 450). 2003 Edition. Part 1: Provisions, Building Seismic Safety Council, National Institute of Building Sciences, Washington, D.C. https://doi.org/10.1614/WS-D-11-00148.1.

Chamoli B.P., Kumar A., Chen D.-Y., Gairola A., Jakka R.S., Pandey B., Kumar P., Rathore G., 2019. A Prototype Earthquake Early Warning System for Northern India. J. Earthq. Eng., 0, 1-19. https://doi.org/10.1080/13632469.2019.1625828.

Dal Moro G., 2019. Effective Active and Passive Seismics for the Characterization of Urban and Remote Areas: Four Channels for Seven Objective Functions. Pure Appl. Geophys, 176, 1445-1465. https://doi.org/10.1007/s00024-018-2043-2.

Dimri V.P., 2013. Uttarakhand had early warning communication in 1894 ! Curr. Sci., 105, 152.

Douglas J., Boore D.M., 2011. High-frequency filtering of strong-motion records. Bull. Earthq. Eng., 9, 395-409. https://doi.org/10.1007/s10518-010-9208-4.

Field E.H., Jacob K.H., 1995. A comparison and test of various site response estimation techniques, including three that are not reference site dependent. Bull. Seismol. Soc. Am., 85, 1127-1143.

Ghasemi H., Zare M., Fukushima Y., Sinaeian F., 2009. Applying empirical methods in site classification, using response spectral ratio (H/V): A case study on Iranian strong motion network (ISMN). Soil Dyn. Earthq. Eng., 29, 121-132. https://doi.org/10.1016/j.soildyn.2008.01.007.

Harinarayan N.H., Kumar A., 2018a. Seismic Site Classification of Recording Stations in Tarai Region of Uttarakhand, from Multiple Approaches. Geotech. Geol. Eng., 36, 1431-1446. https://doi.org/10.1007/s10706-017-0399-1.

Harinarayan N.H., Kumar A., 2018b. Determination of NEHRP Site Class of Seismic Recording Stations in the Northwest Himalayas and Its Adjoining Area Using HVSR Method. Pure Appl. Geophys., 175, 89-107. https://doi.org/10.1007/s00024-017-1696-6.

Havskov J., Alguacil G., 2015. Instrumentation in earthquake seismology, Springer Dordrecht. https://doi.org/10.1007/978-3-319-21314-9.

Japan Road Association, 2002. Design Specification for Highway Bridges, Part V: Seismic Design, Maruzen Co., LTD., Tokyo.

Ji K., Ren Y., Wen R., 2017. Site classification for National Strong Motion Observation Network System (NSMONS) stations in China using an empirical H/V spectral ratio method. J. Asian Earth Sci., 147, 79-94. https://doi.org/10.1016/j.jseaes.2017.07.032.

JRA, 1980. Japan Road Associztion, Specifications for Highway Bridges Part V, Seismic Design, Maruzen Co., LTD. https://doi.org/10.1142/9789812704252_0014.

Kalkan E., 2016. An automatic P-phase Arrival-Time Picker. Bull. Seismol. Soc. Am., 106, 971-986. https://doi.org/10.1785/0120150111.

Konno K., Ohmachi T., 1998. Ground-motion characteristics estimated from spectral ratio between horizontal and vertical components of microtremor. Bull. Seismol. Soc. Am., 88, 228-241. https://doi.org/10.1080/00905992.2016.1248385.

Kumar A., Mittal H., Sachdeva R., 2012. Indian Strong Motion Instrumentation Network. Seismol. Res. Lett., 83, 59-66. https://doi.org/10.1785/gssrl.83.1.59.

Kumar P., Chamoli, B.P., Kumar, A., Gairola, A., 2021. Attenuation Relationship for Peak Horizontal Acceleration of Strong Ground Motion of Uttarakhand Region of Central Himalayas. Journal of Earthquake Engineering, 25(12), 2537-2554. Doi: 10.1080/13632469.2019.1634161.

Langston C.A., 1979. Structure Under Mount Rainier, Washington, Inferred From Teleseismic Body Waves. J. Geophys. Res., 84, 4749-4762. https://doi.org/10.1097/00007611-197001000-00009

Lee C.-T., Cheng C.-T., Liao C.-W., Tsai Y.-B., 2001. Site Classification of Taiwan Free-Field Strong-Motion Stations. Bull. Seism. Soc. Am., 91(5), 1283-1297.

Macau A., Benjumea B., Gabas A., Figueras S., Vila M., 2014. The Effect of Shallow Quaternary Deposits on the Shape of the H/V Spectral Ratio. Surv. Geophys., 36, 1-24. https://doi.org/10.1007/s10712-014-9305-z.

Mittal H., Kumar A., Kumar A., 2013. Site Effects Estimation in Delhi from the Indian Strong Motion Instrumentation Network. Seismol. Res. Lett., 84, 33-41. https://doi.org/10.1785/0220120058.

Mittal H., Kumar A., Ramhmachhuani R., 2012. Indian National Strong Motion Instrumentation Network and Site Characterization of Its Stations. Int. J. Geosci., 03, 1151-1167. https://doi.org/10.4236/ijg.2012.326117.

Mridula Amita S., Wason H.R., 2014. Probabilistic seismic hazard assessment in the vicinity of MBT and MCT in western Himalaya. Res. Inven. Int. J. Eng. Sci., 4, 21-34.

Nakamura Y., 2008. On the H/V Spectrum, in: The 14 World Conference on Earthquake Engineering October 12-17, 2008, Beijing, China. Beijing, 1-10.

Nakamura Y., 1989. A Method for Dynamic Characteristics Estimation of Subsurface using Microtremor on the Ground Surface, Railway Technical Research Institute/Tetsudo Gijutsu Kenkyujo. Railway Technical Research Institute/Tetsudo Gijutsu Kenkyujo, TOKYO, Japan.

New Zealand Standard, 2004. Structural design actions Part 5: Earthquake actions - New Zealand. NZS 1170.5, 1-87.

Pandey B., 2018. Site Characterization and Attenuation studies for Northern India (doctoral thesis). Indian Institute of Technology Roorkee, Roorkee, India.

Pandey B., Jakka R.S., Kumar A., Sharma M.L., 2021. Site characterization of strong-motion stations of Himalaya and adjoining plains. Arab. J. Geosci., 14, 1-21. https://doi.org/https://doi.org/10.1007/s12517-021-07231-y.

Perron V., Gélis C., Froment B., Hollender F., Bard P.Y., Cultrera G., Cushing E.M., 2018. Can broad-band earthquake site responses be predicted by the ambient noise spectral ratio? Insight from observations at two sedimentary basins. Geophys. J. Int., 215, 1442-1454. https://doi.org/10.1093/GJI/GGY355.

Phillips W.S., Aki K., 1986. Site Amplification of Coda Waves from Local Earthquakes in Central California. Bull. Seismol. Soc. Am., 76, 627-648.

Satoh T., Kawase H., Matsushima S., 2001. Differences between site characteristics obtained from microtremors, S-waves, P-waves, and codas. Bull. Seismol. Soc. Am., 91, 313-334. https://doi.org/10.1785/0119990149.

Sharma J., Chopra S., Roy K.S., 2014. Estimation of Source Parameters, Quality Factor (Qs), and Site Characteristics Using Accelerograms : Uttarakhand Himalaya Region. Bull. Seismol. Soc. Am., 104, 360-380. https://doi.org/10.1785/0120120304.

Spearman C., 2010. The proof and measurement of association between two things. Int. J. Epidemiol., 39, 1137-1150. https://doi.org/10.1093/ije/dyq191.

Srivastava H.N., Verma M., Bansal B.K., Sutar A.K., 2015. Discriminatory characteristics of seismic gaps in Himalaya. Geomatics, Nat. Hazards Risk, 6, 224-242. https://doi.org/10.1080/19475705.2013.839483

UBC, 1994. Uniform Building Code, Structural Engineering Design Provisions, Volume 2, International Conference of Building Officials, 5360 Workman Mill Road Whittier, California 90601-2298, 310, 699-0541.

Wen K.-L, Beresnev I.A., Yeh Y.T., 1995. Investigation of non-linear site amplification at two downhole strong ground motion arrays in Taiwan. Earthq. Eng. Struct. Dyn., 24, 313-324. https://doi.org/10.1002/eqe.4290240302.

Wen K.L., Chang T.M., Lin C.M., Chiang H.J., 2006. Identification of nonlinear site response using the H/V spectral ratio method. Terr. Atmos. Ocean. Sci., 17, 533-546. https://doi.org/10.3319/TAO.2006.17.3.533(T).

Wen R., Ren Y., Shi D., 2011. Improved HVSR site classification method for free-field strong motion stations validated with Wenchuan aftershock recordings. Earthq. Eng. Eng. Vib., 10, 325-337. https://doi.org/10.1007/s11803-011-0069-x.

Yamazaki F., Ansary M.A., 1997. Horizontal-To-Vertical Spectrum Ratio of Earthquake Ground Motion for Site. Earthq. Eng. Struct. Dyn., 26(7), 671-689. https://doi.org/10.1002/(SICI)1096-9845(199707)26.

Yu Y., Hu Y., Wang S., 2000. Calculation of Long-Period Ground Motion Response Spectrum by Using Broad-Band Digital Record, in: 12WCEE, 1-7.

Zare M., Bard P.Y., Ghafory-Ashtiany M., 1999. Site characterizations for the Iranian strong motion network. Soil Dyn. Earthq. Eng., 18, 101-123. https://doi.org/10.1016/S0267-7261(98)00040-2.

Zhao J.X., Irikura K., Zhang J., Fukushima Y., Somerville P.G., Asano A., Ohno Y., Oouchi T., Takahashi T., Ogawa H., 2006. An empirical site-classification method for strong-motion stations in Japan using H/V response spectral ratio. Bull. Seismol. Soc. Am., 96, 914-925. https://doi.org/10.1785/0120050124.

Zhao J.X., Irikura K., Zhang J., Fukushima Y., Somerville P.G., Asano A., Saiki T., Okada H., Takahashi T., 2004. Site Classification for Strong-Motion Stations in Japan using H/V Response Spectral Ratio. 13th World Conf. Earthq. Eng. Vancouver, B.C., Canada, August 1-6, 1278p.